



# Experimental characterisation and modelling of the strain rate dependent mechanical response of a filled thermo-reversible supramolecular polyurethane

H. Chen<sup>a</sup>, L.R. Hart<sup>b</sup>, W. Hayes<sup>b</sup>, C.R. Siviour<sup>a,\*</sup>

<sup>a</sup> Solid Mechanics and Materials Engineering, Department of Engineering Science, University of Oxford, Oxford OX1 3PJ, United Kingdom

<sup>b</sup> Department of Chemistry, University of Reading, Reading RG6 6UR, United Kingdom

## ARTICLE INFO

### Keywords:

Supramolecular polyurethanes  
Viscoelasticity  
Filler reinforcement  
Debonding  
High-strain rates

## ABSTRACT

Composites consisting of a polymer binder filled with various particles are widely used in industrial applications, and key to their engineering design is the ability to produce mechanical models of these materials. One limitation of many composites is the use of cross-linked elastomers as matrix materials, which reduces re-usability and recyclability. In this research, a recently developed reusable and low temperature processable supramolecular polyurethane was mixed with sugar particles to produce a model composite material with different particle sizes or volume fractions, which were subsequently characterised and modelled. Large strain mechanical properties of the material were analysed in compression at strain rates up to approximately  $1800 \text{ s}^{-1}$ , supported by measurements of the small strain viscoelastic response at different temperatures and frequencies. A model was developed that combined the known viscoelastic response of the supramolecular polyurethane with filler reinforcement and strain activated damage equations calibrated against quasi-static experiments. The model provided a good prediction of the high strain rate behaviour, for which the effect of adiabatic heating in the sample was also considered. The model parameters were related back to the filler particle size and volume fraction. Finally, a preliminary study of geometry and strength recovery was performed.

## 1. Introduction

Recent research has led to the development of synthetic, healable materials composed of supramolecular polyurethanes (SPUs) which are able, at relatively low temperatures, to recover their topology and mechanical properties when damaged [1–6]. These polymers have advantages of low-temperature processability, low density, biocompatibility and ductility; however, their low moduli at ambient temperature present challenges for use in load-bearing structures [7] and biomedical applications [8]. Over the last few decades, particulate-filled polymers, made by embedding rigid particles into polymer matrices have attracted great scientific interest and enabled access to specific applications [9–11], such as tyres, insulation coatings and packing materials, by improving properties such as stiffness and toughness compared to the polymer alone. Furthermore, fillers can be used to introduce desired functionalities such as thermal conductivity [12,13], electrical conductivity [14], or magnetic performance [15]. Common mechanical modifiers include clay [16], carbon-black [17], fumed silica [18] or two-dimensional

fillers such as nano-tubes, flakes and fibers [19]. The overall mechanical properties of the composite can depend on the filler size [20,21], filler shape [22,23], filler distribution, alignment [24–26], geometric orientation [24], and interfacial adhesion between filler and matrix [27–31]. Another purpose of mixing particulates in a soft polymer is to take advantage of the filler's functionality; for example, in polymer bonded explosives or propellants [32–34], where the role of the polymer binder is to make the explosive system more resilient and less sensitive during processing and transportation [35–38].

Mechanical experiments in tension, compression or bending are conventionally used to characterise basic composite properties. More complex investigations such as microscopy, spectroscopy and scattering [39] are used to investigate structural evolution [40–43] but these observations must then be linked to the overall mechanical response, which can be challenging. Internal mechanical responses, such as interfacial failure [44,45] and fracture [46,47], can depend on the nature of the filler itself [48,49], the composition [50] and the loading situation (e.g. impact [35,51,52], ballistic [53,54], fracture testing [55,

\* Corresponding author.

E-mail address: [clive.siviour@eng.ox.ac.uk](mailto:clive.siviour@eng.ox.ac.uk) (C.R. Siviour).

<https://doi.org/10.1016/j.ijimpeng.2022.104239>

Received 8 November 2021; Received in revised form 6 April 2022; Accepted 7 April 2022

Available online 9 April 2022

0734-743X/© 2022 The Author(s). Published by Elsevier Ltd. This is an open access article under the CC BY license (<http://creativecommons.org/licenses/by/4.0/>).

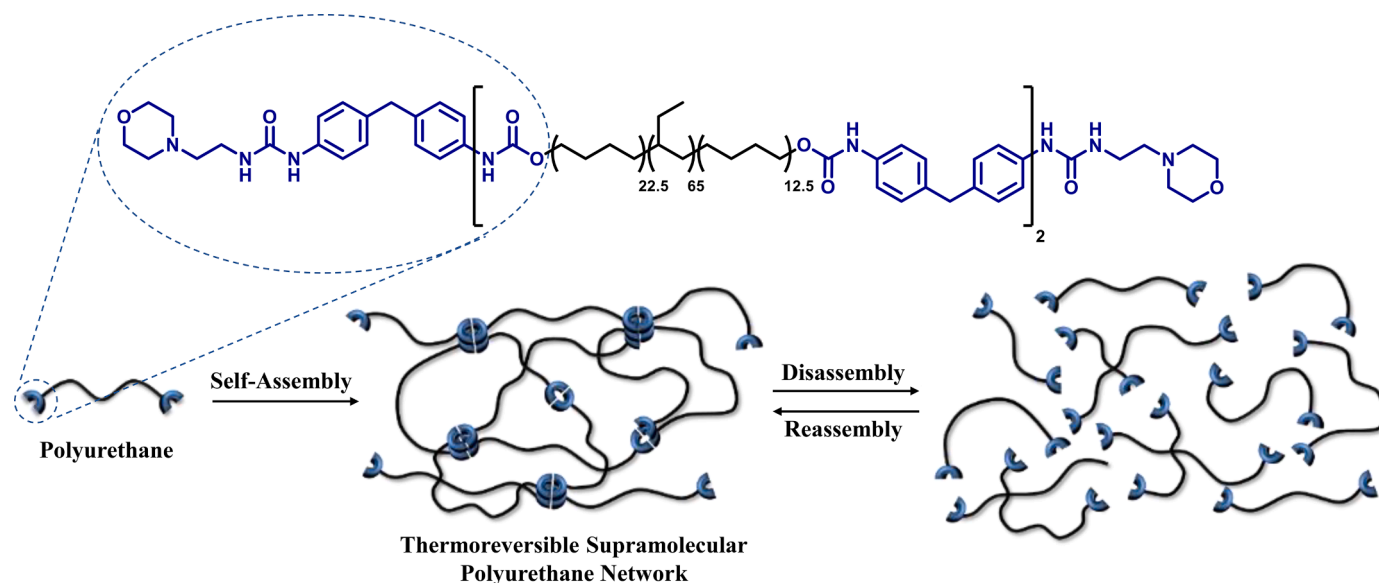


Fig. 1. The healable supramolecular polyurethane, featuring urea morpholine end groups [1]

56]). The development of simple models that link the structure of the composite to its mechanical responses are of importance for effectively utilising these materials in industry and science, and this is the subject of this paper. Additionally, the mechanical properties at high strain rates were determined, and a simple model calibrated from low rate data was used to predict these behaviours. The conventional method for high strain rate characterisation is the split-Hopkinson pressure bar [57]. This has previously been employed to understand mechanical behaviour of similar filled polymers [35,58,59]; however, there are physical limitations for testing low modulus materials at high strain rates [60,61]. The natural frequency of oscillation of the specimen and the effects of specimen inertia both lead to additional forces that mask the underlying specimen response. Further, for materials that deform at low stresses, it is difficult to accurately measure the forces supported by the specimen using a metallic transmission bar as a result of weak transmitted signals, compared to the background noise [62]. To ensure that the properties of the specimen are truly representative of the material response, the specimen needed to be loaded uniformly (i.e. in static stress equilibrium). However, the characteristic low wave speeds in low modulus specimens can result in non-equilibrated stresses causing non-uniform deformation in the specimen (i.e. specimen yielding before dynamic stress equilibrium), which would invalidated the results obtained [63]. Finally, whilst high-speed imaging can be used to monitor deformation and composite failure [64–67], it is not possible to observe microstructural evolution in high strain rate experiments. Hence, there is a requirement for approaches that combine experiments and modelling in order to link low and high strain rate data, with the ultimate aim of better understanding the behaviour under high-rate conditions.

Here, we characterise and model a particulate composite combining a SPU binder with sugar fillers. As well as being inert and non-toxic, the use of sugar has the advantage that it is possible to produce specimens with various, but relatively well-controlled, particle sizes and filler loadings. We propose a combined modelling method based on a predictive model for the SPU behaviour [68]. This was combined with models for the modulus enhancement owing to the filler, and the subsequent strength reduction during loading as the filler debonds from the polymer matrix [35,69]. The modelling procedure started with a viscoelastic polymer model (VPM) for the SPU, characterising the behaviour up to large strains and over a range of strain rates [68]. This model has the advantage of all the parameters being derived from standard rheological and low-rate experiments. The modulus of the composite was then derived using Guth's reinforcement equation [70].

The damage equation is described using a typical phenomenological model for debonding, with parameters that fit to compression stress-strain data, and which can be related to filler volume fraction and particle size. The model was applied to composites with different compositions, deformed over a range of strain rates up to  $1800 \text{ s}^{-1}$ . For modelling high-rate behaviour, the adiabatic heating effect was also incorporated [71]. The model implementations and experimental results in this paper therefore provide an applicable methodology for interpreting the mechanical behaviour of particulate-filled polymers. We have previously shown that the polymer matrix has ability to recover mechanical properties [1,35], therefore, the recovery in these composites was also investigated.

## 2. Material and experimental method

### 2.1. Synthesis of SPU

The polymer binder selected (Fig. 1) has previously been reported [1] to exhibit healable characteristics, however, it does not possess sufficient mechanical strength or stiffness to be useful in many applications where structural integrity is key. To explore the need to reinforce these types of functional materials to increase their utility, the SPU was prepared using a known procedure<sup>1</sup> before formulating composites for analysis. The SPU was synthesized by reacting a non-polar polymeric diol, namely Krasol™ HLBH-P2000, with 4,4'-methylene diphenyl diisocyanate (4,4'-MDI) at  $80^\circ\text{C}$  under argon for three hours to install isocyanate end-groups. 4-(2-Aminoethyl)morpholine was then introduced to decorate the telechelic polymer with polar recognition motifs as end-groups via urea bond formation. The resulting SPU possessed hydrophilic domains (urethanes and ureas recognition motifs) in addition to a hydrophobic polymer back-bone which gave rise to a phase separated morphology. Crucially, this morphology resulted in the formation of a self-assembled network via non-covalent hydrogen bonding and aromatic  $\pi$ - $\pi$  stacking interactions. As a consequence of the reversible supramolecular interactions, the SPU exhibited low temperature processability, excellent adhesion, healability, reusability and biocompatibility [1]. Furthermore, a model for rheological behaviour was presented and a constitutive viscoelastic polymer model was proposed for its compression loading behaviour at strain rates up to  $1200 \text{ s}^{-1}$ .

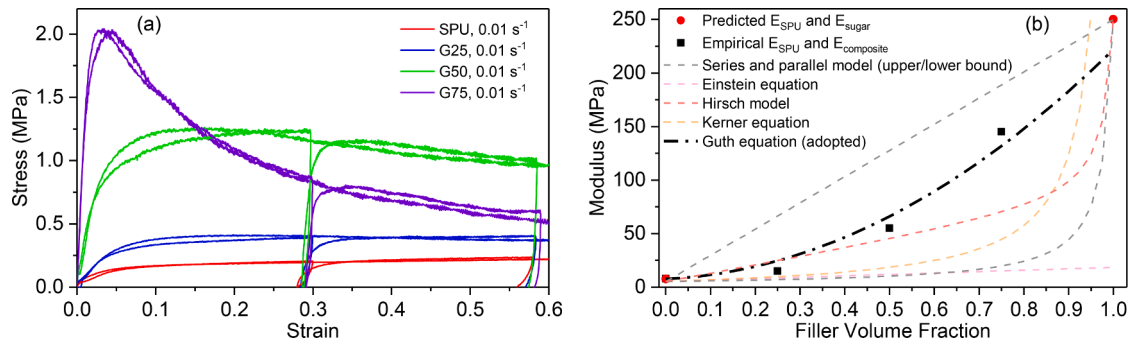


**Fig. 2.** (a) Stress-strain data for filled and unfilled SPU tested in monotonic and cyclic compression experiments at a strain rate of  $0.01 \text{ s}^{-1}$  and  $25^\circ\text{C}$ . The apparent Young's modulus is  $7.2 \text{ MPa}$  for the unfilled polymer and  $15$ ,  $55$  and  $145 \text{ MPa}$  for filled polymer specimens G25, G50 and G75, respectively. The empirical reinforcement factor,  $R_{\text{test}}$  is calculated as  $2.1$ ,  $7.6$  and  $20.1$ . These ratio values can be optimally fitted by the Guth equation when  $P = 3.9$ , and give  $R_{\text{Guth}}$  as  $3.2$  (G25),  $8.5$  (G50) and  $16.8$  (G75). The predicted Young's modulus from the viscoelastic polymer model at  $0.01 \text{ s}^{-1}$  is about  $7.5 \text{ MPa}$  for unfilled SPU, gives predicted Young's moduli for G25, G50 and G75 composites about  $24$ ,  $64$  and  $126 \text{ MPa}$ . Parameters used in other reinforcement equations are:  $v_m = 0.49$  for Kerner equation;  $E_p = 250 \text{ MPa}$  for the series and parallel model;  $x = 0.3$  for the Hirsch model.

## 2.2. Particulate composite: sugar-filled SPU

The sugar-filled polymer specimens for compression experiments were prepared and moulded individually. Three types of sugar particles (Tate & Lyle Ltd, UK) were used: granulated ( $530\text{--}670 \mu\text{m}$ ), caster ( $270\text{--}340 \mu\text{m}$ ) or icing ( $20\text{--}25 \mu\text{m}$ ) sugars; micrographs of the sugar fillers for these three categories are shown in Fig. SI-1 the product specification [72] for particle sizes is also given in Table SI-1. The density of sugar,  $\rho_f$ , is  $1600 \text{ kg m}^{-3}$  [73]. To produce the composite, the appropriate amount of sugar was immersed into the molten polymer at  $80^\circ\text{C}$ ; the resulting mixture was slowly, mixed and extruded to avoid grinding or crushing the sugar particle, and preventing air voids becoming trapped inside the specimens. The mixture was then gently injected into a PTFE mould (Fig. SI-2) from which cylindrical specimens were prepared of diameter  $6.35 \pm 0.1 \text{ mm}$  and length  $7.4 \pm 0.1 \text{ mm}$ . Various filler loading densities were prepared; for granulated sugar, these were  $25$ ,  $50$ ,  $70$  and  $75\%$  (referred to hereon as: G25, G50, G70 and G75) by volume; for caster sugar  $50$  and  $65\%$  (C50 and C65) and for icing sugar  $30$  and  $50\%$  (I30 and I50). In order to confirm that the specimens were prepared to the correct composition, their densities were calculated and compared to the theoretical density before experiments which were in good agreement; see Table SI-2 for an example.

## 2.3. Low- and high-rate compression experiments

Low-rate compression experiments were performed in a commercial screw-driven load frame (Instron 5980) using an environmental chamber to maintain a constant temperature of  $25^\circ\text{C}$ . The specimen was centered between two loading anvils and compressed under true strain rate control at  $0.01 \text{ s}^{-1}$ . The load cell had a measurement capacity of  $1 \text{ kN}$ . Force and deformation records from the crosshead were used to calculate the true stress-strain response, assuming that the deformation took place at constant volume. Specimens of composites G25, G50, G75, C50, C65, I30, I50 were tested at a true strain rate of  $0.01 \text{ s}^{-1}$ , composite G50 was also tested at  $0.001$  and  $0.1 \text{ s}^{-1}$  in order to understand the rate dependence. After the compression experiments, some specimens were held at a constant temperature of  $37^\circ\text{C}$ , in order to observe their shape recovery.

In order to characterise the response to high strain rate deformation, up to  $1800 \text{ s}^{-1}$ , high rate experiments were performed using a Split-Hopkinson pressure bar (SHPB) [57,60,74,75] at room temperature ( $20^\circ\text{C}$ ). In this experiment, a cylindrical specimen is placed between the ends of two titanium alloy bars. A third bar, known as a striker, is accelerated in a gas gun until it impacts the incident bar. The impact creates an 'incident' stress wave that travels along the bar to the specimen. At the bar-specimen interface, the wave is partially reflected along

the incident bar and partially transmitted through specimen. The incident, reflected and transmitted waves were measured by strain gauges on the incident and transmission bars. These measurements were used to calculate the stress equilibrium, deformation rate and surface force at the bar-specimen interfaces, from which the true strain-stress behaviour in the specimen is determined [57,62].

## 3. Modelling and experimental results

### 3.1. Polymer model – viscoelastic theory

The SPU polymer matrix was modelled using a viscoelastic method described in a previous paper [68]. The model was assembled from an empirical Maxwell model combined with an additional dashpot: the former was parameterized by a Prony series that used empirical thermal-mechanical data from rheometry and DMA experiments in the principle of time-temperature superposition; the latter was defined to allow the whole model to fit the empirical rate-dependence. The overall model enables the large strain response to be described in compression up to  $\sim 1200 \text{ s}^{-1}$ . The model construction and simulations were executed in Simscape® (Simulink, Matlab®). In this paper, the model was again used for the mechanical behaviour of the unfilled SPU over a range of strain rates and was combined with a particle reinforcement equation and a damage equation to describe the composite behaviour, assigning as the viscoelastic polymer model.

### 3.2. Filled polymer – moduli reinforcement

There has been significant interest in the mechanical response of particle-filled polymers [70,76–81]. One of the earliest theories for a composite system with rigid spherical inclusions was based on Einstein's equation; further models, all described in the SI, include the Kerner equation [78], the series and parallel model [79], and the Hirsch model [80]. The model used in this paper is Guth's reinforcement equation (RE) [70]; here the composite stiffness is calculated as:

$$E_{c,0} = E_{m,0} \left( 1 + 0.67PV_f + 1.62P^2V_f^2 \right), \quad (1)$$

where  $E_{m,0}$  is the modulus of the matrix and  $V_f$  is the volume fraction of particles.  $P$  is nominally the aspect ratio for non-spherical particles, but here is treated as a fitting parameter to obtain the correct reinforcement for different volume fractions. In this paper, we define the ratio,  $R_{\text{Guth}} = E_{c,0} / E_{m,0}$ , as a reinforcement factor that increases the modulus of the polymer matrix to that of the composite at the same strain rate and temperature conditions. To characterise  $P$ , empirical data from specimens of unfilled SPU, G25, G50 and G75, tested in compression at a

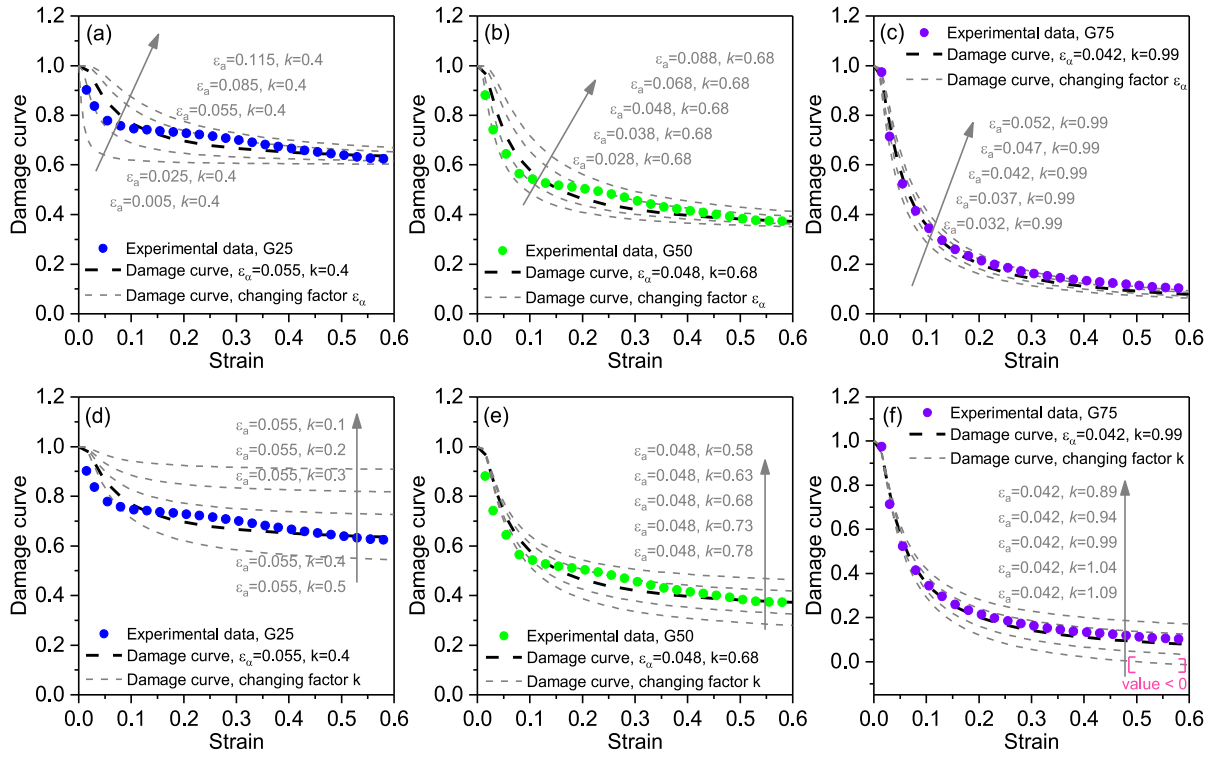


Fig. 3. Damage curve using damage Eq. 5 with different values of  $\epsilon_a$  and  $k$ . The empirical damage was determined by  $E_{\text{secant, test}} / (E_m \times R_{\text{Guth}})$ , where  $E_m$  is the local secant modulus determined by the viscoelastic polymer model.

strain rate of  $0.01 \text{ s}^{-1}$ , were used, shown in Fig. 2a. The apparent Young's moduli (i.e. initial compression moduli) were extracted and fitted to all the above formulations with appropriate values of  $E_{m,0}$ ,  $E_c$ ,  $\sigma_0$

and  $V_f$ . Fig. 2b shows a comparison of the models with the experimental data, indicating that the Guth equation with  $P = 3.9$  afforded the best fit.

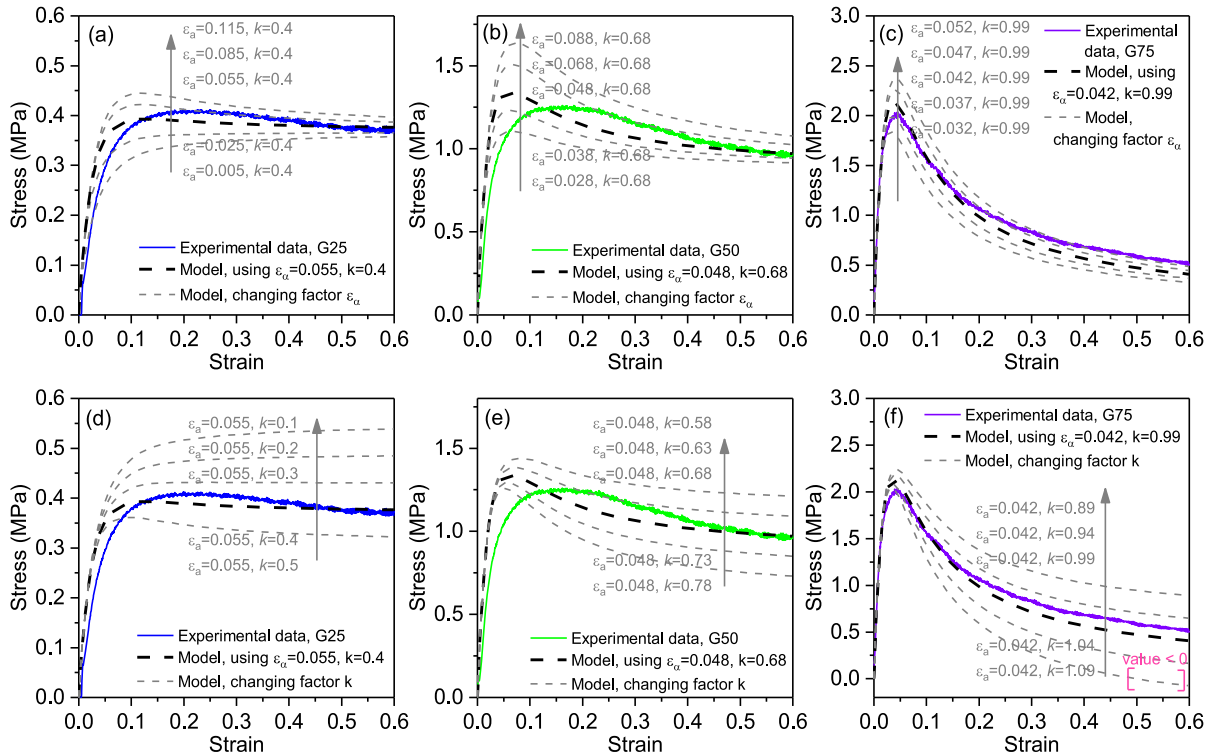
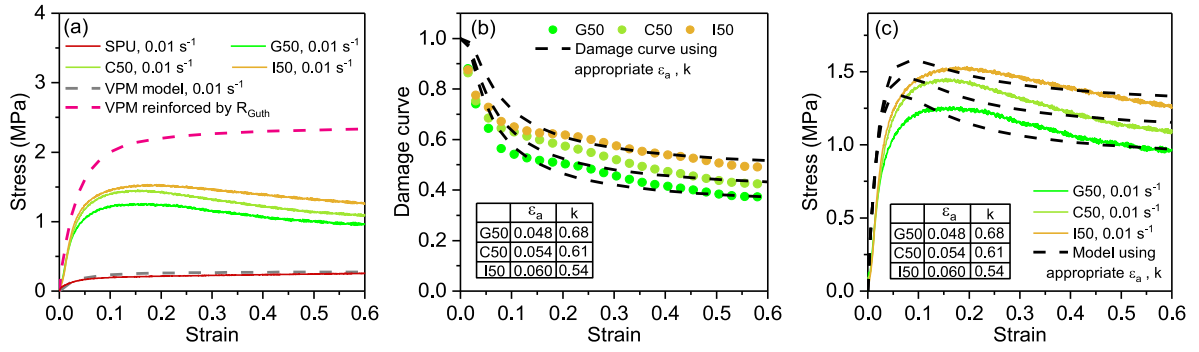


Fig. 4. Strain-stress behaviour modelled using damage Eq. 5 with different values of  $\epsilon_a$  and  $k$ . The ultimate stress was determined via  $\sigma = E \cdot \epsilon$ . The best-fitting parameters  $R_{\text{Guth}}$ ,  $\epsilon_a$ ,  $k$ , for the modelling of the composite behaviour at  $0.01 \text{ s}^{-1}$  and  $25^\circ\text{C}$  were assigned as follows G25: 3.2, 0.055, 0.4; G50: 8.5, 0.048, 0.68; G75: 16.8, 0.042, 0.99.





**Fig. 5.** Model implementation for specimens of G50, C50 and I50, in which (a) the Guth reinforcement equation was used to reinforce the viscoelastic polymer model, (b) the damage equation with optimal value of  $\varepsilon_a$  and  $k$  from Eq. 5 was used to perform (c) modelling of the composite behaviour at  $0.01 \text{ s}^{-1}$  and  $25^\circ\text{C}$ . The parameters  $R_{\text{Guth}}$ ,  $\varepsilon_a$ ,  $k$  were assigned as G50: 8.5, 0.048, 0.68; C50: 8.5, 0.054, 0.61; I50: 8.5, 0.06, 0.54.

### 3.3. Composite model – continuum damage model

The strength of the filled polymer is dominated by the structural integrity of the filler-matrix interface [35,58]. The debonding surrounds individual crystals at small strains, and forms micro-cracks as the strain increases, resulted in strain softening in the constitutive response [59, 82]. This is consistent with the observed behavior of crystals debonding from the binder reported by Siviour *et al.* [35]. Li *et al.* [83] observed interface debonding of matrix and particles as the main form of damage at small stress, while at higher stresses micro-cracks along the boundary of crystals and transgranular fracture through crystals developed. Ravindran *et al.* reported [51] localized shear in polymer rich areas and in crystals that experience fracture, indicating another phenomenon of failure evolution. Computational simulations have also been employed [84–86], to verify the initiation of failure in interfacial debonding.

Building on previous research [35], the overall damage is modelled here by degrading the modulus using a function similar in form to the Weibull distribution [87]. The development of the model is described here. In the previous research, an activation strain,  $\varepsilon_a$ , which is dependent on the filler particle size, was used to parameterize the debonding according to

$$E = E_{c,0} \left[ 1 - \exp \left( - \left( \frac{\varepsilon_a}{\varepsilon} \right)^2 \right) \right] \quad (2)$$

$$E_{c,0} = R_{\text{Guth}} \times E_{m,0} \quad (3)$$

$$\sigma = E \cdot \varepsilon \quad (4)$$

where  $E_{c,0}$  is the Young's modulus of the intact composite predicted using the Guth equation multiplying the Young's modulus of the

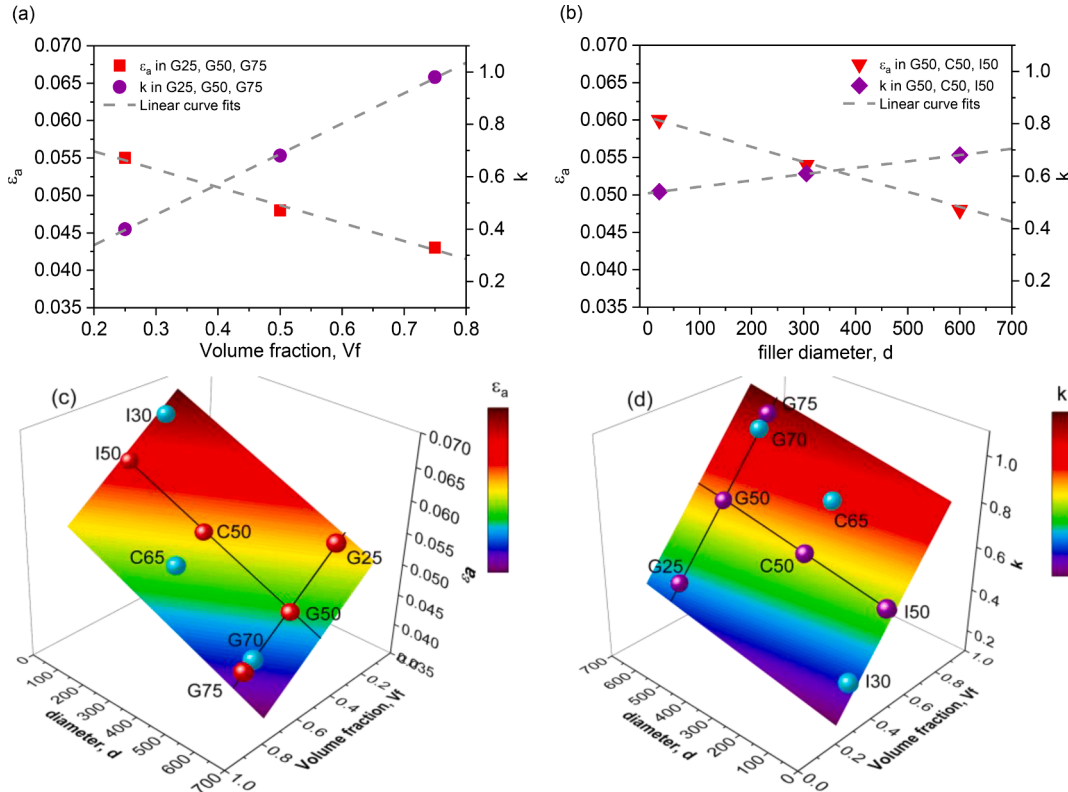


**Fig. 6.** (a) and (b) show the linear relations between fitting parameters  $\varepsilon_a$ ,  $k$  and filler particle size and volume fraction. These two 2D plots correspond to 3D surfaces (c) and (d). From surface plots (c) and (d), a unique set of damage parameters can be extracted for any particle diameter and volume fraction. For example, the parameters  $R_{\text{Guth}}$ ,  $\varepsilon_a$ ,  $k$  were assigned to specimens of I30, C65 and G70 as: I30: 4, 0.065, 0.31; C65: 13, 0.051, 0.78; G70: 14.9, 0.043, 0.93.

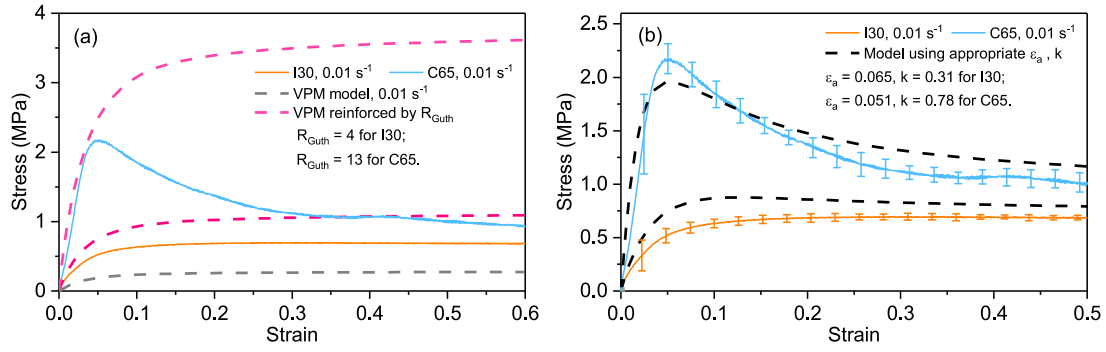


**Fig. 7.** Model implementation for specimens of I30 and C65. (a) Comparison of model with Guth reinforcement equation, but no damage, to the experimental data; (b) comparison of full model with damage to the experimental data. The parameters,  $R_{Guth}$ ,  $\epsilon_a$ ,  $k$ , were assigned as I30: 4, 0.065, 0.31; C65: 13, 0.051, 0.78, to model the behaviour at 0.01 s<sup>-1</sup> and 25°C.

polymer,  $E_{m,0}$ , from the viscoelastic polymer model.  $R_{Guth}$  is the ratio value, calculated from Fig. 2. The value of  $\epsilon_a$  was fit to the experimental data to determine the stress. The model outputs are given in Supplementary Information (Figs SI-3 and SI-4). The limitation of using this constitutive model was because it over-estimates the post-yield softening behaviour.

A number of modifications to the damage equations were made (see SI). The final expression used is as follows:

$$E = E_c \left[ 1 - k \exp\left(-\frac{\epsilon_a}{\epsilon}\right) \right], \quad (5)$$

where an additional parameter  $k$  was added to represent the material maintaining strength at high strains. The effects of the two parameters for the model on both the damage ratio and the resulting stress-strain curves are presented in more detail in Figs. 3 and 4. Here, the activation strain,  $\epsilon_a$ , dominates the initial modulus and position of the peak stress, whilst  $k$  adjusts the behaviour at larger strains.

### 3.4. Further model parametrization and parameter comparisons

The model was fitted to a series of experiments with different particle sizes. In all cases, the viscoelastic polymer model was first used to predict the behaviour of the matrix at each strain rate; then the stress-strain curve was modified using the appropriate reinforcement factor according to the specific filler loadings. Finally, the stress-strain curve thus produced was compared to the empirical data for the same material, to produce a damage factor as a function of strain. Again, parameters  $\epsilon_a$  and  $k$  were fitted. Fig. 5 shows equivalent data from specimens with a fixed volume fraction but different particle sizes: G50, C50 and I50.

The values of  $\epsilon_a$  and  $k$  obtained were then plotted against the microstructural parameters of filler diameter,  $d$ , and filler loading,  $V_f$ , Fig. 6. In both cases, the relation was observed to be linear, allowing a

3D plane surface to be plotted for each of the two model parameters. From this surface, values of  $\epsilon_a$  and  $k$  can now be estimated for a specific composition.

To verify the parametrization, additional compression experiments were performed on materials with different compositions: Icing Sugar with volume fraction 30% (I30) and Caster Sugar with volume fraction 65% (C65), again at 25°C and 0.01 s<sup>-1</sup>. The required parameters,  $\epsilon_a$  and  $k$ , were extracted from the 3D surface plots in Fig. 6. The full empirical datasets for specimens I30 and C65 are shown in Fig. SI-14. A comparison of the models to experimental data is presented in Fig. 7.

### 3.5. Model application for low- to high-rate behaviour

Data from further experiments on G50, G70 and G75, and the corresponding models, are used to validate the model application to both low and high strain rate behavior. To capture the experiments with different loading rates, the viscoelastic polymer model at the same ambient temperatures and strain rates was assigned. To respond to temperature changes, the principle of time-temperature superposition was employed: a master curve of modulus was produced at a new shifted reference temperature, and this curve was used to build a new set of Prony series parameters [68]. This allowed the predicted constitutive behaviour for unfilled SPU at the specific reference temperature to be determined, whilst the values of  $R_{Guth}$ ,  $\epsilon_a$  and  $k$  determined above were employed. For compositions that were yet untested, the relevant parameters were assigned by extracting values from 2D/3D mapping plots in Fig. 6.

Results from quasi-static experiments and the equivalent models for specimen G50 at 0.001, 0.01 and 0.1 s<sup>-1</sup> are shown in Fig. 8 (the full set of experimental data is shown in Fig. SI-15). The model was able to accurately reproduce the observed behaviour. For higher rate data up to 1800 s<sup>-1</sup>, the same implementation was applied, Fig. 9. Fig. 10 describes

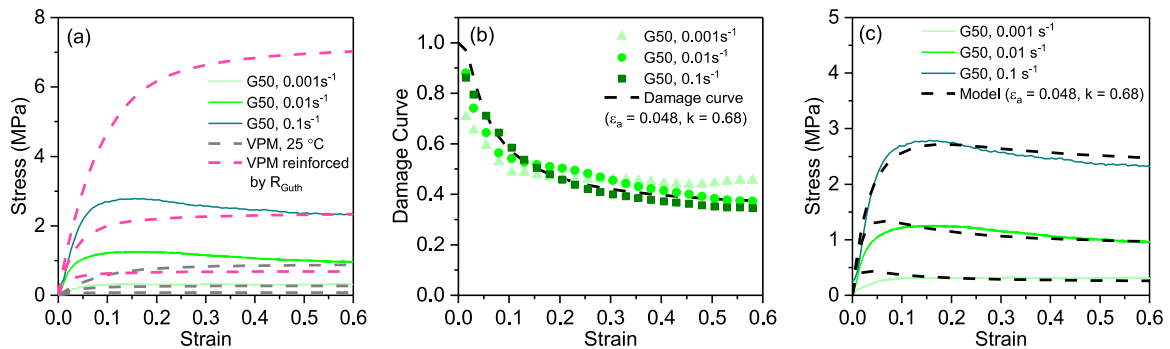


**Fig. 8.** Model implementation for specimen G50, in which (a) the Guth reinforcement equation was used to reinforce the viscoelastic polymer model, (b) the damage parameters  $\epsilon_a$  and  $k$  were used to model the composite behaviour (c) from 0.001 to 0.01 s<sup>-1</sup> and 25°C. The parameters,  $R_{Guth}$ ,  $\epsilon_a$ ,  $k$  were same as Fig. 3, assigned as G50: 8.5, 0.048, 0.68.

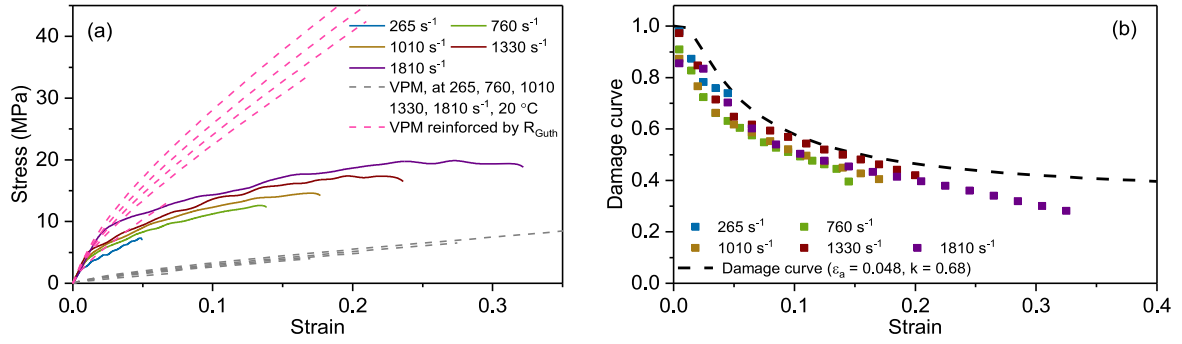


**Fig. 9.** Model implementation for specimen G50, in which (a) the Guth reinforcement equation was used to reinforce the viscoelastic polymer model, (b) the damage parameters  $\varepsilon_a$  and  $k$  from the quasi-static experiments (Figs. 3-4) were used.

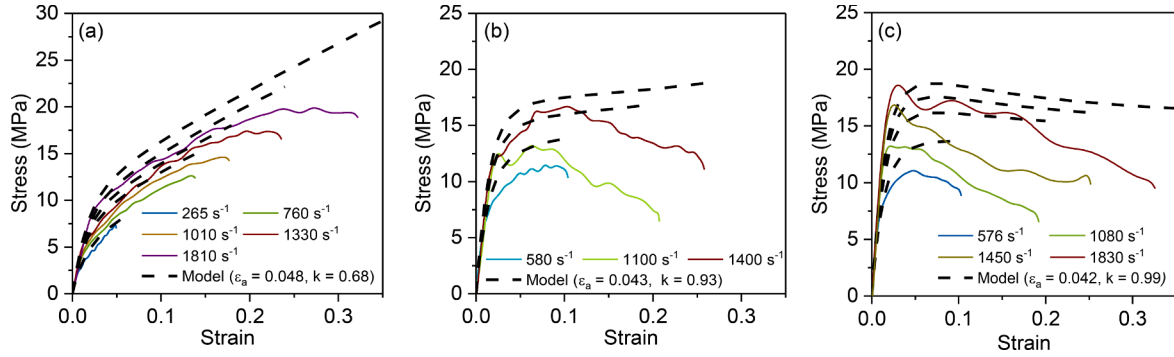


**Fig. 10.** Model implementation for specimen (a) G50, (b) G70 and (c) G75. The implementation of Guth reinforcement equation and the damage model are introduced in Figs. 9, SI-20 and SI-21. The parameters,  $R_{Guth}$ ,  $\varepsilon_a$ ,  $k$  were assigned as G50: 8.5, 0.048, 0.68; G70: 14.9, 0.043, 0.93, determined from Fig. 6; G75: 16.8, 0.042, 0.99. It is noticed that parameters from the quasi-static experiments (Figs. 3-4) were used to model G50 and G75 in high rates.

the model captures well the initial stiffness and subsequent behaviour at small strains (full data in Figs SI-16 to SI-18); however, the stress was overestimated at large strains compared to the empirical data. Although it is possible to optimally fit the experimental data and thus improve the model fittings by using an alternative set of parameters (see Fig. SI-19), this reduced the predictive capability of the viscoelastic polymer model and the utilization of parameters from quasi-static experiments; it also removed the correspondence to composite composition. A second approach to achieve better fitting at high strain rates was to consider the effect of adiabatic heating to reduce the stress at large deformations.

### 3.6. Modelling of adiabatic heating effects

Viscoelastic or plastic deformation of the specimen converts work into heat. In high strain rate experiments, this causes a temperature rise in the specimen, as there is insufficient time for this heat to conduct into

the loading bars: the experiment takes place in adiabatic thermal conditions. This temperature rise may affect the subsequent deformation of the polymer, and hence affect the stress-strain behaviour, especially at large deformation. Fig. SI-22 demonstrates the effect of temperature rises on the behaviour of the polymer, this is somewhat amplified when considering the composite. In terms of adiabatic heating, the temperature rise as a function of strain can be approximately calculated as:

$$\Delta T(\varepsilon) = \frac{\beta}{\rho C_p} \int_0^\varepsilon \sigma d\varepsilon, \quad (6)$$

where  $\sigma$  is the true stress,  $\varepsilon$  the true strain,  $\rho = 950 \text{ kg m}^{-3}$  the material density,  $C_p = 1850 \text{ J kg}^{-1} \text{ K}^{-1}$  the specific heat capacity of the polymer, measured from a DSC experiment, and  $\Delta T$  represents the rise in temperature;  $\beta$  represents the fraction of work converted to heat during the deformation [71]. This is only an approximate calculation because  $\beta$  is not known, and the distribution of heat between the matrix and particles

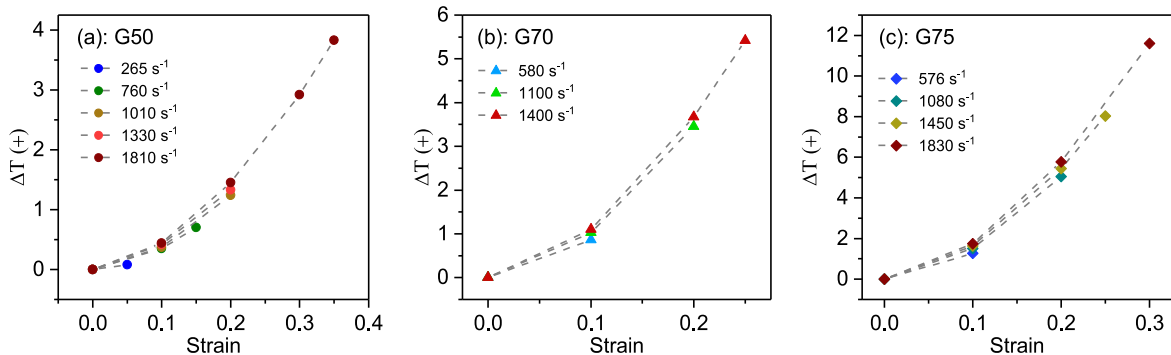


**Fig. 11.** The temperature rise predicted at strain intervals of 0.1 in composites of G50, G70 and G75, in adiabatic conditions.

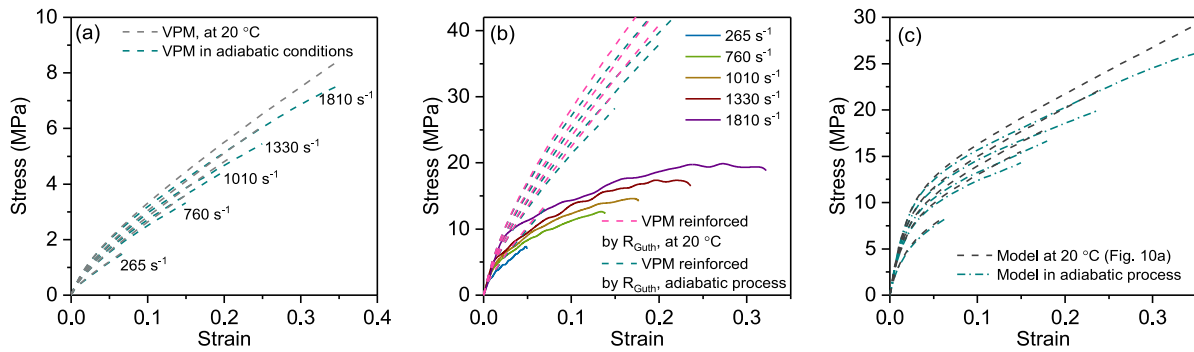


**Fig. 12.** Model implementation for specimen G50: the ‘new’ viscoelastic polymer model with adiabatic heating effects was compared to previous polymer model (a); the Guth reinforcement equation was used to reinforce the ‘new’ viscoelastic polymer model (b); the same damage parameters  $\varepsilon_a$  and  $k$  was used (c), to compare the ‘new’ model outputs with previous data.

is not considered.

In order to verify the degree of impact of adiabatic heating on the composite stress at large deformations, an extreme case was considered at large deformation and high rates. First, the maximum conversion rate,  $\beta = 1$ , was used to represent the work done being fully transferred into heat. Secondly, all the deformation was assumed to be adopted within the polymer matrix (see Fig. SI-23), for instance in the G50 specimen the strain rate in the SPU matrix twice the overall (applied) rate. This increase of strain rate in the matrix would be larger (i.e. likely three to four times higher) in specimens of G70 and G75. Using this latter assumption gives the polymer stress-strain curves in Fig. SI-24. Thirdly, the overall strain was divided into several regular intervals, at the end of which the heat generation was calculated. This approach was adopted so that the time-temperature superposition (TTS) master-curve only had to be recalculated a limited number of times. Here a strain interval of 0.1 was used in most cases; at each interval step a new stress-strain curve was calculated towards the new raised temperature; the determination of temperature rise at each step can be reviewed in Tables SI-3 to SI-5, Fig. SI-25. A summary of temperature rises for the steps is shown in Fig. 11.

Using these assumptions, the predicted rises in temperature for specimens of G50, G70 and G75 were about 4 to 11 °C. This heating is assumed to cause a change in the mechanical response of the polymer as a result of increased mobility of the chains, but not in  $R_{Guth}$ ,  $\varepsilon_a$  and  $k$  or the sugar response. It is noted that, in fact  $\varepsilon_a$  is likely to change, as the interaction and adhesion between the matrix and filler changes when polymer matrix becomes more viscous, but it was assumed that this is not significant in this study.

Plots of the viscoelastic polymer model output at each calculated temperature are given in Figs SI-26 to SI-28. These were then used to derive the viscoelastic behaviour during a continuous heating process, shown in Fig. 12a, SI-29a and SI-30a for specimens of G50, G70, G75, respectively. New strain-stress plots under the assumption of continuous adiabatic heating, after reinforcement by the Guth equation, are given in Figs 12b, SI-29b and SI-30b. The ultimate stress-strain behaviours of composites G50, G70 and G75 with adiabatic heating effects are illustrated in the rest Fig. 12. These data show that including the adiabatic heating effect leads to a small improvement in the model, but does not fully remove the discrepancy between model and experiment. It was interesting to investigate the effect of incorporating these increased strain rates into the overall mechanical model of the polymer, this is discussed further in the SI.

### 3.7. Strain recovery of SPU-based composites

The SPU matrix used in these composites has been shown to partially recover its geometry after deformation [11]; an investigation into strain recovery, and behaviour on reloading, of the filled composites was also performed. The test specimens were prepared as described previously,

loaded in quasi-static compression at a constant true strain rate of  $0.01 \text{ s}^{-1}$ . The temperature was controlled at 25 °C during compression, and at 37 °C in the recovery periods after each test. Specimens of SPU, G25, G50, C50, I50 and G75 were investigated so that the effects of particle size and volume fraction could be observed. Raw data of strain recovery against time are given in Fig. SI-36, stress-strain data produced when re-testing the specimens after recovery can be reviewed in Fig. SI-37. Fig. 14 shows logarithmic strain recovery against time. It is observed that this shows a linear dependence with a gradient that depends on the composition of the material. These gradients are then linked to the volume fraction or filler diameter.

Further compression experiments were performed to assess the stress-strain behaviour of samples under cyclic loading in which the second loading took place immediately, and after three hours recovery (see Fig. SI-37). Although there is significant geometric recovery in many of the specimens, the strength was similar in both cases.

## 4. Discussion and conclusions

The research presented here characterised low- and high-rate mechanical behaviour of sugar-filled SPU composites. Specimens were manufactured consisting of an SPU matrix and fillers of granulated, caster or icing sugar particles with different filler loadings. A practical modelling method was proposed, which builds on the fundamental viscoelastic polymer model for the unfilled polymer to model the behaviour of sugar-filled SPU composites via progressive reinforcement and damage equations. Several reinforcement and damage models were introduced, and the optimal equation combination was adopted. Assigning appropriate parameters into the equations, the model was able to represent the properties of composites tested in quasi-static compression. The same modelling procedure and parameters from quasi-static experiments were then used to model high-rate experiments, in order to validate the use of both the viscoelastic model and the damage equation. For composites which had not yet been tested in low-rate experiments, the determination of their parameters for modelling were obtained from a set of phenomenological 3D surface plots which associated the parameters with filler size and volume fraction. The effect of adiabatic heating to reduce the stress in the high-rate experiments was taken into account in order to optimize the agreement of the model with empirical data.

The modelling procedure began with a constitutive viscoelastic polymer model from the literature [68]. Several filler reinforcement models were introduced: Guth’s equation, Kerner’s equation and Hirsch’s equation. Guth’s equation was chosen as the best of these equations. The match between the equation and the results is not perfect; this may be a result of scatter in the experimental results or distribution of particle sizes.

Three damage equations, based on the formulation of the Weibull distribution, were proposed. Full simulation results were computed, and



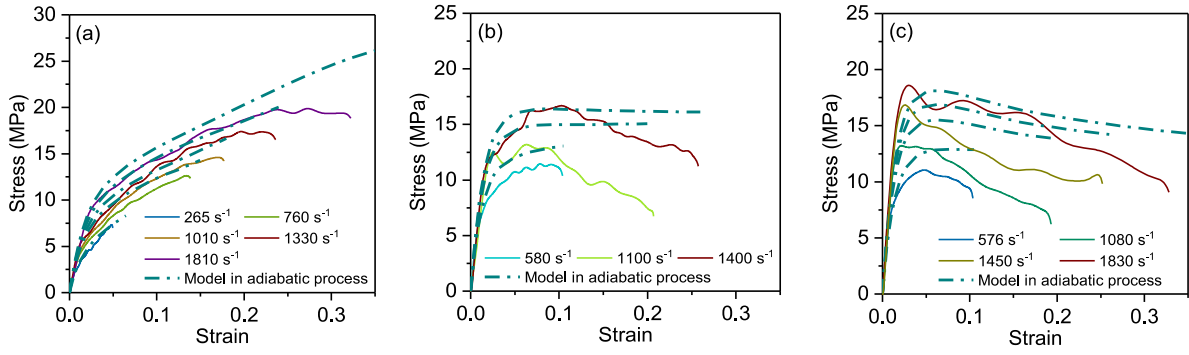


**Fig. 13.** Model implementation for specimen (a) G50, (b) G70 and (c) G75. The ‘new’ viscoelastic polymer model with adiabatic heating effects, the Guth reinforcement equation and further damage model implementations were illustrated in Figs. 12, SI-29 and SI-30. The modelling of the composite behaviour performed at  $0.01 \text{ s}^{-1}$  and  $20^\circ\text{C}$ . The parameters,  $R_{Guth}$ ,  $\epsilon_a$ ,  $k$  were as follows: G50: 8.5, 0.048, 0.68; G70: 14.9, 0.043, 0.93; G75: 16.8, 0.042, 0.99.

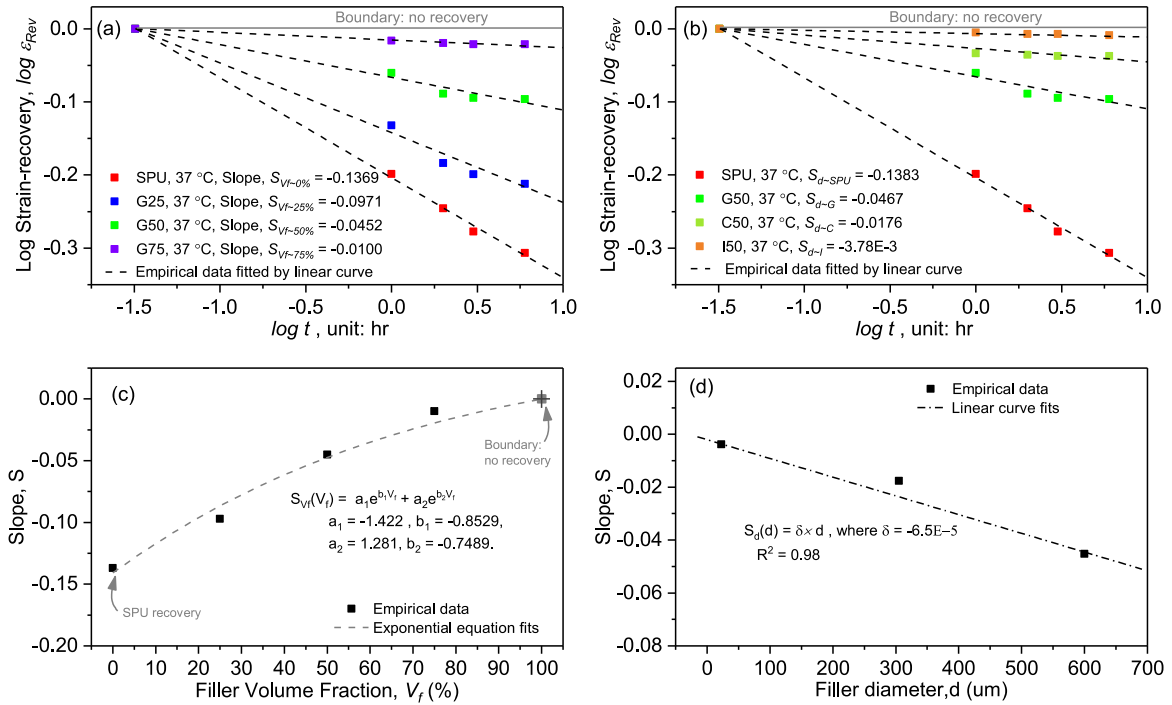


**Fig. 14.** Strain recovery in specimens (a) SPU, G25, G50, G75 (b) SPU, G50, C50, I50 at  $37^\circ\text{C}$ . The gradient of the logarithmic recovery is plotted against volume fraction (c) and filler size (d).

the damage equation led to the best fit to empirical data was chosen. The chosen equation uses two parameters, an activation energy to describe damage, assumed to be caused by debonding of the particles from the matrix,  $\epsilon_a$ , and a second parameter  $k$ , representing the residual strength of the material. Unlike previous models in the literature, the underlying rate and temperature dependent polymer behaviour was retained by degrading the secant modulus of the filled polymer (which is equivalent to multiplying the stress-strain curve for the polymer by the damage factor).

For materials already tested in low-rate experiments, parameters can be determined, then used to predict mechanical behaviour at different rates. For materials without pre-assigned parameters, a mapping of parameters,  $\epsilon_a$  and  $k$  to filler size and volume fraction provided a good prediction. Further, the model was capable of modelling rate dependence in the material, albeit with less accuracy at very high strain rates. Errors and discrepancies might be seen as a result of specimen preparation, errors in the reinforcement factor or the parameter estimation. Further errors from the viscoelastic polymer model might be expected at higher rates, where the rate dependence is larger and the model is

therefore more sensitive to small changes in rate and therefore to errors in the measured strain rates. The model parameters could also be fit to the high-rate data, providing an improvement here at the expense of predictive capability.

The potential effect of adiabatic heating on the model output was also considered, this provides a small improvement in the model output compared to the experimental results. However, the new model stress outputs are still over-estimated, e.g. by 20% for G50 at the highest rate and strain (Fig. 13a), compared to the empirical values at very large strain. This is possibly because the damage scenarios were different between quasi-static experiments and high-rate impact experiments. From the literature [88,89], it is known that when stress or strain is small, the debonding mechanism is predominant, while at large stresses, fracture might appear in both the filler and the matrix rich area. This may occur preferentially at high strain rates, because the stresses are higher, and would accelerate the damage process and reduce the empirical strain-stress behaviour compared to the model. There may also be non-uniform deformation (e.g. shear bands) in high rate experiments, and the filler-matrix interface may be sensitive to polymer

properties in a manner that affects the high rate behaviour.

The recoveries of strain and stress during cyclic loadings were briefly investigated. A logarithmic recovery of strain with time was evolved, with the rate of recovery depending on the particle size and volume fraction. The recovery of strength was minimal in these specimens; however, it is likely that this would be improved if they were allowed to recover in more confined conditions, or for longer.

In conclusion, this study on sugar-filled SPU polymers characterised their properties at quasi-static and high strain rates for different filler types and loading proportions. The modelling procedure built up a clear concept of using a predictive unfilled polymer model combined with a reinforcement equation and damage model to produce a practicable modelling procedure for the overall material using the viscoelastic polymer model and composition information from the composites.

## CRediT authorship contribution statement

**H. Chen:** Investigation, Methodology, Data curation, Conceptualization, Writing – review & editing. **L.R. Hart:** Formal analysis, Writing – review & editing. **W. Hayes:** Resources, Formal analysis, Writing – review & editing. **C.R. Siviour:** Resources, Conceptualization, Project administration, Supervision, Writing – review & editing.

## Declaration of Competing Interest

The authors declare that they have no known competing financial interests or personal relationships that could have appeared to influence the work reported in this paper.

## Acknowledgements

The authors would like to thank Air Force Office of Scientific Research, Air Force Material Command, USAF under Award Nr. FA9550-15-1-0448. We also thank EPSRC (EP/N024818/1) for post-doctoral research fellowship in support of LRH. We also would like to thank Igor Dyson for technical support at Oxford University.

## Supplementary materials

Supplementary material associated with this article can be found, in the online version, at [doi:10.1016/j.ijimpeng.2022.104239](https://doi.org/10.1016/j.ijimpeng.2022.104239).

## References

- [1] Feula A, Tang X, Giannakopoulos I, Chippindale AM, Hamley IW, Greco F, et al. An adhesive elastomeric supramolecular polyurethane healable at body temperature. *Chem Sci* 2016;7:4291–300. <https://doi.org/10.1039/C5SC04864H>.
- [2] Huang WM, Yang B, Zhao Y, Ding Z. Thermo-moisture responsive polyurethane shape-memory polymer and composites: a review. *J Mater Chem* 2010;20:3367–81. <https://doi.org/10.1039/B922943D>.
- [3] Rivero G, Nguyen L-TT, Hillewaere XKD, Du Prez FE. One-pot thermo-remendable shape memory polyurethanes. *Macromolecules* 2014;47:2010–8. <https://doi.org/10.1021/ma402471c>.
- [4] Feula A, Pethybridge A, Giannakopoulos I, Tang X, Chippindale A, Siviour CR, et al. A Thermoreversible Supramolecular Polyurethane with Excellent Healing Ability at 45 °C. *Macromolecules* 2015;48:6132–41. <https://doi.org/10.1021/acs.macromol.5b01162>.
- [5] Petrović ZS, Ferguson J. Polyurethane elastomers. *Prog Polym Sci* 1991;16:695–836. [https://doi.org/10.1016/0079-6700\(91\)90011-9](https://doi.org/10.1016/0079-6700(91)90011-9).
- [6] Koberstein JT, Galambos AF, Leung LM. Compression-molded polyurethane block copolymers. 1. Microdomain morphology and thermomechanical properties. *Macromolecules* 1992;25:6195–204. <https://doi.org/10.1021/ma00049a017>.
- [7] Salimi S, Hart LR, Feula A, Hermida-Merino D, Touré ABR, Kabova EA, et al. Property enhancement of healable supramolecular polyurethanes. *Eur Polym J* 2019;118:88–96. <https://doi.org/10.1016/j.eurpolymj.2019.05.042>.
- [8] Ramakrishna S, Mayer J, Wintermantel E, Leong KW. Biomedical applications of polymer-composite materials: a review. *Compos Sci Technol* 2001;61:1189–224. [https://doi.org/10.1016/S0266-3538\(00\)00241-4](https://doi.org/10.1016/S0266-3538(00)00241-4).
- [9] Rothern R. Particulate-filled polymer composites. iSmithers Rapra Publishing; 2003.
- [10] Rothern R. Fillers for polymer applications. Berlin, Germany: Springer; 2017.
- [11] DeArmitt C, Rothern R. Particulate fillers, selection and use in polymer composites. *Encycl Polym Compos* 2015;2017:1–19.
- [12] Lee G-W, Park M, Kim J, Lee JI, Yoon HG. Enhanced thermal conductivity of polymer composites filled with hybrid filler. *Compos Part A Appl Sci Manuf* 2006;37:727–34. <https://doi.org/10.1016/j.compositesa.2005.07.006>.
- [13] Huang X, Jiang P, Tanaka T. A review of dielectric polymer composites with high thermal conductivity. *IEEE Electr Insul Mag* 2011;27:8–16. <https://doi.org/10.1109/MEI.2011.5954064>.
- [14] Bhadra S, Rahman M, Khanam PN. Electrical and electronic application of polymer-carbon composites. Carbon-containing Polym. Compos. 2019:397–455. [https://doi.org/10.1007/978-981-13-2688-2\\_12](https://doi.org/10.1007/978-981-13-2688-2_12).
- [15] Xu C, Lin M, Wang X, Shen Q, Zheng Z, Lin B, et al. Fabrication of high-performance magnetic elastomers by using natural polymer as auxiliary dispersant of Fe3O4 nanoparticles. *Compos Part A Appl Sci Manuf* 2021;140:106158. <https://doi.org/10.1016/j.compositesa.2020.106158>.
- [16] Rao Y, Pochan JM. Mechanics of polymer-clay nanocomposites. *Macromolecules* 2007;40:290–6. <https://doi.org/10.1021/ma061445w>.
- [17] Ojha S, Acharya SK, Raghavendra G. Mechanical properties of natural carbon black reinforced polymer composites. *J Appl Polym Sci* 2015;132. <https://doi.org/10.1002/app.41211>.
- [18] Mora-Barrantes I, Rodríguez A, Ibarra L, González L, Valentín JL. Overcoming the disadvantages of fumed silica as filler in elastomer composites. *J Mater Chem* 2011;21:7381–92. <https://doi.org/10.1039/C1JM10410A>.
- [19] Saba N, Tahir PM, Jawaid M. A review on potentiality of nano filler/natural fiber filled polymer hybrid composites. *Polymers (Basel)* 2014;6:2247–73. <https://doi.org/10.3390/polym6082247>.
- [20] Vollenberg PHT, Heikens D. Particle size dependence of the Young's modulus of filled polymers: 1. Preliminary experiments. *Polymer (Guildf)* 1989;30:1656–62. [https://doi.org/10.1016/0032-3861\(89\)90326-1](https://doi.org/10.1016/0032-3861(89)90326-1).
- [21] Fu S-Y, Feng X-Q, Lauke B, Mai Y-W. Effects of particle size, particle/matrix interface adhesion and particle loading on mechanical properties of particulate-polymer composites. *Compos Part B Eng* 2008;39:933–61. <https://doi.org/10.1016/j.compositesb.2008.01.002>.
- [22] Samal S. Effect of shape and size of filler particle on the aggregation and sedimentation behavior of the polymer composite. *Powder Technol* 2020;366:43–51. <https://doi.org/10.1016/j.powtec.2020.02.054>.
- [23] Singh SS, Parameswaran V, Kitey R. Dynamic compression behavior of glass filled epoxy composites: Influence of filler shape and exposure to high temperature. *Compos Part B Eng* 2019;164:103–15. <https://doi.org/10.1016/j.compositesb.2018.11.061>.
- [24] Cooper CA, Ravich D, Lips D, Mayer J, Wagner HD. Distribution and alignment of carbon nanotubes and nanofibrils in a polymer matrix. *Compos Sci Technol* 2002;62:1105–12. [https://doi.org/10.1016/S0266-3538\(02\)00056-8](https://doi.org/10.1016/S0266-3538(02)00056-8).
- [25] Chen W, Tao X. Self-organizing alignment of carbon nanotubes in thermoplastic polyurethane. *Macromol Rapid Commun* 2005;26:1763–7. <https://doi.org/10.1002/marc.200500531>.
- [26] Xie X-L, Mai Y-W, Zhou X-P. Dispersion and alignment of carbon nanotubes in polymer matrix: a review. *Mater Sci Eng R Reports* 2005;49:89–112. <https://doi.org/10.1016/j.mser.2005.04.002>.
- [27] Verbeek CJR. The influence of interfacial adhesion, particle size and size distribution on the predicted mechanical properties of particulate thermoplastic composites. *Mater Lett* 2003;57:1919–24. [https://doi.org/10.1016/S0167-577X\(02\)01105-9](https://doi.org/10.1016/S0167-577X(02)01105-9).
- [28] Jin L, Wang H, Yang Y. Polyurethane composites in situ molecularly reinforced by supramolecular nanofibrillar aggregates of sorbitol derivatives. *Compos Sci Technol* 2013;79:58–63. <https://doi.org/10.1016/j.compscitech.2013.02.017>.
- [29] Habibpour S, Um JG, Jun Y, Bhargava P, Park CB, Yu A. Structural impact of graphene nanoribbon on mechanical properties and anti-corrosion performance of polyurethane nanocomposites. *Chem Eng J* 2021;405:126858. <https://doi.org/10.1016/j.cej.2020.126858>.
- [30] Olonakis K, Fan M, Xin-Xiang Z, Ran L, Lin W, Zhang W, et al. Key Improvements in Interfacial Adhesion and Dispersion of Fibers/Fillers in Polymer Matrix Composites. Focus on PLA Matrix Composites. *Compos Interfaces* 2021:1–50. <https://doi.org/10.1080/09276440.2021.1878441>.
- [31] Li T, Meng Z, Ketten S. Interfacial mechanics and viscoelastic properties of patchy graphene oxide reinforced nanocomposites. *Carbon N Y* 2020;158:303–13. <https://doi.org/10.1016/j.carbon.2019.10.039>.
- [32] Daniel MA. Polyurethane binder systems for polymer bonded explosives. 2006. <https://doi.org/10.1016/j.jieec.2014.05.004>.
- [33] Lee S, Choi JH, Hong I-K, Lee JW. Curing behavior of polyurethane as a binder for polymer-bonded explosives. *J Ind Eng Chem* 2015;21:980–5.
- [34] Ahmed T late AE-SI, Ali AA, El-Masry AM, Tawfik SM. Development of Polyurethane-Based Solid Propellants Using Nanocomposite Materials. *Propellants, Explos Pyrotech* 2016;41:286–94. <https://doi.org/10.1002/prep.201500182>.
- [35] Siviour CR, Laity PR, Proud WG, Field JE, Porter D, Church PD, et al. High strain rate properties of a polymer-bonded sugar: their dependence on applied and internal constraints. *Proc R Soc A Math Phys Eng Sci* 2008;464:1229–55. <https://doi.org/10.1098/rspa.2007.0214>.
- [36] Kendall MJ, Siviour CR. Experimentally simulating high rate composite deformation in tension and compression: polymer bonded explosive simulant. *J Dyn Behav Mater* 2015;1:114–23. <https://doi.org/10.1007/s40870-015-0018-2>.
- [37] Huang X, Huang Z, Lai J-C, Li L, Yang G-C, Li C-H. Self-healing improves the stability and safety of polymer bonded explosives. *Compos Sci Technol* 2018;167:346–54. <https://doi.org/10.1016/j.compscitech.2018.08.025>.
- [38] Budd ME, Stephens R, Afsar A, Salimi S, Hayes W. Exploiting thermally-reversible covalent bonds for the controlled release of microencapsulated isocyanate

- crosslinkers. *React Funct Polym* 2019;135:23–31. <https://doi.org/10.1016/j.reactfunctpolym.2018.12.008>.
- [39] Sadasivuni KK, Ponnammam D, Kumar B, Strankowski M, Cardinaels R, Moldenaers P, et al. Dielectric properties of modified graphene oxide filled polyurethane nanocomposites and its correlation with rheology. *Compos Sci Technol* 2014;104:18–25. <https://doi.org/10.1016/j.compscitech.2014.08.025>.
- [40] Du W, Liu J, Wang Y, Li Y, Li Z. Polyurethane encapsulated carbon black particles and enhanced properties of water polyurethane composite films. *Prog Org Coatings* 2016;97:146–52. <https://doi.org/10.1016/j.porgcoat.2016.04.006>.
- [41] Maganty S, Roma MPC, Meschter SJ, Starkey D, Gomez M, Edwards DG, et al. Enhanced mechanical properties of polyurethane composite coatings through nanosilica addition. *Prog Org Coatings* 2016;90:243–51. <https://doi.org/10.1016/j.porgcoat.2015.10.016>.
- [42] Jenczyk J, Woźniak-Budych M, Jancelewicz M, Jarek M, Jurga S. Structural and dynamic study of block copolymer–Nanoparticles nanocomposites. *Polymer (Guildf)* 2019;167:130–7. <https://doi.org/10.1016/j.polymer.2019.01.080>.
- [43] Roy M, Nelson JK, MacCrone RK, Schadler LS, Reed CW, Keefe R. Polymer nanocomposite dielectrics-the role of the interface. *IEEE Trans Dielectr Electr Insul* 2005;12:629–43. <https://doi.org/10.1109/TDEI.2005.1511089>.
- [44] Pukanszky B. Influence of interface interaction on the ultimate tensile properties of polymer composites. *Composites* 1990;21:255–62. [https://doi.org/10.1016/0010-4361\(90\)90240-W](https://doi.org/10.1016/0010-4361(90)90240-W).
- [45] Sadeghpour E, Guo Y, Chua D, Shim VPW. A modified Mori–Tanaka approach incorporating filler-matrix interface failure to model graphene/polymer nanocomposites. *Int J Mech Sci* 2020;180:105699. <https://doi.org/10.1016/j.ijmecsci.2020.105699>.
- [46] Zhuk A V, Knunyants NN, Oshmyan VG, Topolkaev VA, Berlin AA. Debonding microprocesses and interfacial strength in particle-filled polymer materials. *J Mater Sci* 1993;28:4595–606. <https://doi.org/10.1007/BF00414247>.
- [47] Arora H, Tarleton E, Li-Mayer J, Charalambides MN, Lewis D. Modelling the damage and deformation process in a plastic bonded explosive microstructure under tension using the finite element method. *Comput Mater Sci* 2015;110: 91–101. <https://doi.org/10.1016/j.commatsci.2015.08.004>.
- [48] Ferdous SF, Sarker MF, Adnan A. Role of nanoparticle dispersion and filler-matrix interface on the matrix dominated failure of rigid C60-PE nanocomposites: A molecular dynamics simulation study. *Polymer (Guildf)* 2013;54:2565–76. <https://doi.org/10.1016/j.polymer.2013.03.014>.
- [49] Gao Z, Tsou AH. Mechanical properties of polymers containing fillers. *J Polym Sci Part B Polym Phys* 1999;37:155–72. [https://doi.org/10.1002/\(SICI\)1099-0488\(19990115\)37:2<155::AID-POLB5>3.0.CO;2-2](https://doi.org/10.1002/(SICI)1099-0488(19990115)37:2<155::AID-POLB5>3.0.CO;2-2).
- [50] Bréchet Y, Cavaillé J-Y, Chabert E, Chazeau L, Dendievel R, Flandin L, et al. Polymer Based Nanocomposites: Effect of Filler-Filler and Filler-Matrix Interactions. *Adv Eng Mater* 2001;3:571–7. [https://doi.org/10.1002/1527-2648\(200108\)3:8<571::AID-ADEM571>3.0.CO;2-M](https://doi.org/10.1002/1527-2648(200108)3:8<571::AID-ADEM571>3.0.CO;2-M).
- [51] Ravindran S, Tessema A, Kidane A. Multiscale damage evolution in polymer bonded sugar under dynamic loading. *Mech Mater* 2017;114:97–106. <https://doi.org/10.1016/j.mechmat.2017.07.016>.
- [52] Ravindran S, Gupta V, Tessema A, Kidane A. Effect of particle mass fraction on the multiscale dynamic failure behavior of particulate polymer composites. *Exp Mech* 2019;59:599–609. <https://doi.org/10.1007/s11340-019-00493-4>.
- [53] Lee BL, Song JW, Ward JE. Failure of Spectra® polyethylene fiber-reinforced composites under ballistic impact loading. *J Compos Mater* 1994;28:1202–26. <https://doi.org/10.1177/002199839402801302>.
- [54] Lee J-H, Veyssat D, Singer JP, Retzsch M, Saini G, Pezeril T, et al. High strain rate deformation of layered nanocomposites. *Nat Commun* 2012;3:1–9. <https://doi.org/10.1038/ncomms2166>.
- [55] Silva R V, Spinelli D, Bose Filho WW, Neto SC, Chierice GO, Tarpani JR. Fracture toughness of natural fibers/castor oil polyurethane composites. *Compos Sci Technol* 2006;66:1328–35. <https://doi.org/10.1016/j.compscitech.2005.10.012>.
- [56] Wong KJ, Yousif BF, Low KO, Ng Y, Tan SL. Effects of fillers on the fracture behaviour of particulate polyester composites. *J Strain Anal Eng Des* 2010;45: 67–78. <https://doi.org/10.1243/03093247JSA553>.
- [57] Gray III GT, WR Blumenthal. Split-Hopkinson pressure bar testing of soft materials. *ASM Handb* 2000;8:488–96.
- [58] Hu Z, Luo H, Bardenhagen SG, Siviour CR, Armstrong RW, Lu H. Internal deformation measurement of polymer bonded sugar in compression by digital volume correlation of in-situ tomography. *Exp Mech* 2015;55:289–300. <https://doi.org/10.1007/s11340-014-9856-4>.
- [59] Drodge DR, Williamson DM. Understanding damage in polymer-bonded explosive composites. *J Mater Sci* 2016;51:668–79. <https://doi.org/10.1007/s10853-013-7378-6>.
- [60] Siviour CR, Jordan JL. High strain rate mechanics of polymers: a review. *J Dyn Behav Mater* 2016;2:15–32. <https://doi.org/10.1007/s40870-016-0052-8>.
- [61] Song B, Chen W. Split Hopkinson pressure bar techniques for characterizing soft materials. *WwwLajssOrg Lat Am J Solids Struct* 2005;2:113–52.
- [62] Chen WW. Experimental methods for characterizing dynamic response of soft materials. *J Dyn Behav Mater* 2016;2:2–14. <https://doi.org/10.1007/s40870-016-0047-5>.
- [63] Chen W, Lu F, Frew DJ, Forrestal MJ. Dynamic Compression Testing of Soft Materials. *J Appl Mech* 2002;69:214. <https://doi.org/10.1115/1.1464871>.
- [64] Ravindran S, Tessema A, Kidane A. Local deformation and failure mechanisms of polymer bonded energetic materials subjected to high strain rate loading. *J Dyn Behav Mater* 2016;2:146–56. <https://doi.org/10.1007/s40870-016-0051-9>.
- [65] Catalanotti G, Kuhn P, Xavier J, Koerber H. High strain rate characterisation of intralaminar fracture toughness of GFRPs for longitudinal tension and compression failure. *Compos Struct* 2020;240:112068. <https://doi.org/10.1016/j.compstruct.2020.112068>.
- [66] Sassi S, Tarfaoui M, Ben Yahia H. An investigation of in-plane dynamic behavior of adhesively-bonded composite joints under dynamic compression at high strain rate. *Compos Struct* 2018;191:168–79. <https://doi.org/10.1016/j.compstruct.2018.02.057>.
- [67] Koerber H, Xavier J, Camanho PP, Essa YE, De La, Escalera FM. High strain rate behaviour of 5-harness-satin weave fabric carbon–epoxy composite under compression and combined compression–shear loading. *Int J Solids Struct* 2015;54: 172–82. <https://doi.org/10.1016/j.ijsolstr.2014.10.018>.
- [68] Chen H, Hart LR, Hayes W, Siviour CR. Mechanical characterisation and modelling of a thermoreversible superamolecular polyurethane over a wide range of rates. *Polymer (Guildf)* 2021;123607. <https://doi.org/10.1016/j.polymer.2021.123607>.
- [69] Jerabek M, Major Z, Renner K, Móczó J, Pukánszky B, Lang RW. Filler/matrix-debonding and micro-mechanisms of deformation in particulate filled polypropylene composites under tension. *Polymer (Guildf)* 2010;51:2040–8. <https://doi.org/10.1016/j.polymer.2010.02.033>.
- [70] Guth E. Theory of filler reinforcement. *Rubber Chem Technol* 1945;18:596–604.
- [71] Kendall MJ, Siviour CR. Experimentally simulating adiabatic conditions: Approximating high rate polymer behavior using low rate experiments with temperature profiles. *Polym (United Kingdom)* 2013;54:5058–63. <https://doi.org/10.1016/j.polymer.2013.06.049>.
- [72] ASR Group. ASR Group Tate & Lyle Specialty Ingredients. Tate Lyle, UK, Ltd; 2019. [www.sugarandsyrup.com](http://www.sugarandsyrup.com). accessed May 2, 2020.
- [73] ILO and WHO. SUCROSE ICSC: 1507. ICSC 1507 2003. May 5, 2020. [www.ilo.org/dyn/icsc](http://www.ilo.org/dyn/icsc). accessed.
- [74] Siviour CR. High strain rate characterization of polymers. *AIP Conf Proc* 2017; 1793. <https://doi.org/10.1063/1.4971585>.
- [75] Cady CM, Blumenthal WR, Gray III GT, DJ Idar. Mechanical properties of plastic-bonded explosive binder materials as a function of strain-rate and temperature. *Polym Eng Sci* 2006;46:812–9. <https://doi.org/10.1002/pen.20540>.
- [76] Ahmed S, Jones FR. A review of particulate reinforcement theories for polymer composites. *J Mater Sci* 1990;25:4933–42. <https://doi.org/10.1007/BF00580110>.
- [77] Einstein A. Investigations on the Theory of the Brownian Movement. Courier Corporation; 1956.
- [78] Lewis TB, Nielsen LE. Dynamic mechanical properties of particulate-filled composites. *J Appl Polym Sci* 1970;14:1449–71. <https://doi.org/10.1002/app.1970.070140604>.
- [79] Broutman LJ, Krock RH. Modern Composite Materials: Editors: LJ Broutman and RH Krock. Addison-Wesley Publishing Company; 1967.
- [80] Hirsch TJ. Modulus of elasticity of concrete affected by elastic moduli of cement paste matrix and aggregate. *J. Proc.* 1962;59:427–52.
- [81] Anthoulis GI, Kontou E. Micromechanical behaviour of particulate polymer nanocomposites. *Polymer (Guildf)* 2008;49:1934–42. <https://doi.org/10.1016/j.polymer.2008.02.010>.
- [82] Rae PJ, Goldrein HT, Palmer SJP, Field JE, Lewis AL. Quasi-static studies of the deformation and failure of  $\beta$ -HMX based polymer bonded explosives. *Proc R Soc London Ser A Math Phys Eng Sci* 2002;458:743–62. <https://doi.org/10.1098/rspa.2001.0894>.
- [83] Jun-Ling LI, Hua FU, TAN Duo-Wang, Fang-Yun LU, Rong C. Fracture behaviour investigation into a polymer-bonded explosive. *Strain* 2012;48:463–73. <https://doi.org/10.1111/j.1475-1305.2012.00842.x>.
- [84] Yan-Qing W, Feng-Lei H. A micromechanical model for predicting combined damage of particles and interface debonding in PBX explosives. *Mech Mater* 2009; 41:27–47. <https://doi.org/10.1016/j.mechmat.2008.07.005>.
- [85] Wang X, Wu Y, Huang F. Numerical mesoscopic investigations of dynamic damage and failure mechanisms of polymer bonded explosives. *Int J Solids Struct* 2017; 129:28–39. <https://doi.org/10.1016/j.ijsolstr.2017.09.017>.
- [86] Lv L, Yang M, Long Y, Chen J. Molecular dynamics simulation of structural and mechanical features of a Polymer-bonded explosive interface under tensile deformation. *Appl Surf Sci* 2021;557:149823. <https://doi.org/10.1016/j.apsusc.2021.149823>.
- [87] Weibull W. A statistical theory of strength of materials. IVB-Handl 1939.
- [88] Williamson DM, Palmer SJP, Proud WG, Govier R. Brazilian disc testing of a UK PBX approaching the glass transition condition. *AIP Conf. Proc.* 2009;1195:494–7. <https://doi.org/10.1063/1.3295182>.
- [89] Williamson DM, Palmer SJP, Proud WG, Govier R. Brazilian disc testing of a UK PBX above and below the glass transition temperature. *AIP Conf. Proc.* 2007;955: 803–6. <https://doi.org/10.1063/1.2833246>.